Int. J. Heat Mass Transfer. Vol. 15, pp. 1851–1863. Pergamon Press 1972. Printed in Great Britain

EVAPORATION FROM A TWO-DIMENSIONAL EXTENDED MENISCUS

M. POTASH, JR. and P. C. WAYNER, JR.

Division of Fluid, Chemical, and Thermal Processes, Rensselaer Polytechnic Institute, Troy, New York, U.S.A.

(*Received* 16 *September* 1971)

Abstract—The transport processes occurring in an evaporating two-dimensional meniscus and adsorbed thin film formed on a superheated flat glass plate (0·272°C superheat) immersed in a pool of saturated carbon tetrachloride are modeled and analyzed. Fluid flow results from a change in the external meniscus profile. The pressure gradient for fluid flow includes the effect of disjoining pressure. The resulting extended meniscus profile, heat flux profile, and pressure derivative profile are calculated. The presence of an adsorbed superheated film results in a smooth transition between the evaporating and nonevaporating portions of the extended meniscus.

NOMENCLATURE

A, constant in equation (14);
B, constant in equation (14);
c, heat capacity [erg/g°K];
g, gravitational acceleration [cm/s^2];
g_c, conversion factor [cmg/dyne s^2];
h, heat transfer coefficient [W/cm^2 °K]; enthalpy [erg/g]; height above pool [cm];
H, latent heat of evaporation [Ws/g];
J, mechanical equivalent of heat [erg/Ws];
K, curvature [cm^{-1}];
k, thermal conductivity [W/cm°K];
L, distance above bottom of equilibrium thin film [cm];
M, molecular weight [g/mole];
P, modified pressure, $p_g + \rho gh$ [dyne/cm^2];
p, pressure [dyne/cm^2];
Q, heat flux [W/cm^2];
q, heat flow [Ws/g];
Re, Reynolds number, $2\bar{u}\theta r/\nu$;
$\mathscr{R}$, gas constant [erg/mole K°];
R, radius of curvature [cm^{-1}];
r, radial direction (see Fig. 1) [cm];
s, arc length (see Fig. 1) [cm];
s, specific entropy [erg/g °K];
S, arc length (see Fig. 1) [cm];
T, temperature [°K];
t, meniscus thickness [cm];
u, radial velocity [cm/s];
v, specific volume [cm^3/g];
w, mass flux [g/cm^2 s];
x, x co-ordinate (see Fig. 1) [cm];
y, y co-ordinate (see Fig. 1) [cm];
Y, height of evaporating portion of meniscus [cm];
z, distance (see Fig. 1) [cm];
β, derivative of surface tension with respect to temperature [dyne/cm °K];
Δ, difference;
ε, velocity weighting factor [21];
θ, angle (see Fig. 1) [rad];
λ, function of Re and θ, see equation (27);
μ, viscosity [poise];
μ, chemical potential [erg/g];
ν, kinematic viscosity [cm^2/s];
ξ, (φ/θ_i);
ρ, density [g cm^3];
σ, surface tension [dyne/cm];
σ, evaporation coefficient;
τ, stress [dyne/cm^2];

φ, co-ordinate angle (see Fig. 1) [radians];
ζ, pressure function [see equation (22)].

Subscripts

a. atmospheric;
b. base of meniscus;
d. disjoining pressure;
dL. disjoining pressure at L;
g. gage;
h. at location h (see Fig. 1);
i. at location i (see Fig. 1);
L. at location L;
l. liquid;
lh. liquid at h;
lL. liquid at L;
lp. liquid at p;
lv. liquid–vapor interface;
lvo. liquid–vapor interface at o;
lvh. liquid–vapor interface at h;
o. bottom of equilibrium thin film;
p. pool surface;
s. solid;
t. thermodynamic saturation. top of intrinsic meniscus;
v. vapor;
vh. vapor pressure at h;
vlv. vapor pressure at liquid–vapor interface;
vlvo. vapor pressure at liquid–vapor interface at o;
vlvt. saturation vapor pressure at liquid–vapor interface;
vp. saturation vapor pressure at surface of the pool;
1. initial interval;
∞. free stream (liquid–vapor interface).

Overlines

—. average.

INTRODUCTION

INTERFACIAL phenomena in general, and more specifically, those phenomena associated with evaporation from a meniscus play a major role in many current engineering applications which require high local heat fluxes. For example, the evaporating meniscus is one of the limiting parameters in heat pipes, grooved evaporators, fuel cells, suction nucleate boiling devices, and sweat cooling devices. It is likely that the study of the transport processes occurring in an evaporating extended meniscus will prove useful in the improvement of such applications.

For the purposes of this study, the following terms are defined (see Fig. 1): *extended meniscus*

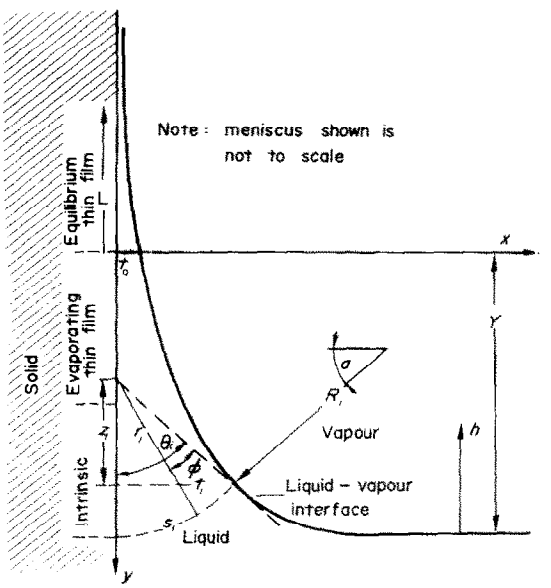

FIG. 1.

—the combined intrinsic meniscus and the thin film extending above it (if present); *intrinsic meniscus*—that portion of the extended meniscus profile which is described by the conventional equation of capillarity

$$\Delta p = \frac{\sigma_{lv}}{R} \tag{1}$$

while excluding the effects of disjoining pressure; *thin films*—that portion of the extended meniscus above the intrisic meniscus.

Many of the phenomena which take place within the evaporating extended meniscus have been the subject of extensive research. The

field of interfacial resistance to mass transfer has been studied both theoretically and experimentally (e.g. [1–4]). Heat transfer in an evaporating meniscus has been studied experimentally [5, 6] and fluid flow in an evaporating intrinsic meniscus has been analyzed using a wedge flow model [7]. The relationships between equilibrium vapor pressure and either temperature or surface curvature are known from the Clausius–Clapeyron and Kelvin equations. The theory of thin film adsorption and disjoining pressure have been explored both theoretically and experimentally [8–12]. A modification to the Kelvin equation has been proposed [8] to account for the effects of disjoining pressure. The dynamics of fluid interfaces is an established field [13]. The Marangoni effect has been investigated [14, 15] and has been shown [7] to be unimportant in a portion of the evaporating meniscus. In a closely related field, the nature of electrolyte films on semi-immersed electrodes, a significant amount of research has been done using a fluid flow model in which the average velocity was assumed to be zero [16–18]. Daryagin *et al.* [19], using adsorption isotherms and the disjoining pressure concept, demonstrated that thin film transport is capable of accelerating by several times the evaporation rate from capillaries.

The net result of the enumerated research is that, while all of the individual phenomena that govern the evaporating meniscus have been actively studied, very little has been done to incorporate all of these phenomena into a model which predicts the behavior of an evaporating extended meniscus. For example, previous work [7] accounted for viscous pressure losses due to the flow of liquid to replenish the evaporated fluid and for the pumping characteristics of the curved surface but did not account for the Marangoni effect, the interfacial resistance due to the mass transfer, and adsorption as described by the disjoining pressure. The objectives of the present study are: (1) Model the transport processes occurring in an evaporating extended meniscus in which the pressure gradient for fluid flow results from both capillarity and disjoining pressure; and (2) using thermodynamic data for the disjoining pressure and the Laplace equation for capillarity, calculate the pressure derivative profile, the heat flux profile, and the extended meniscus profile for a given plate superheat. The analysis includes the effect of interfacial resistance to mass transfer but does not include the Marangoni effect.

QUALITATIVE DESCRIPTION OF AN EXTENDED MENISCUS

This analysis develops the profile of the extended meniscus formed on the surface of a vertical flat plate maintained at a constant temperature, T_s, while one end of the plate is immersed in a pool of liquid at a lower temperature, T_p ($T_p < T_s$). The pure vapor surrounding the plate is saturated at the surface of the pool, has a constant temperature, T_v, and a pressure, p_{vh}, equal at the surface of the pool to its saturation value p_{vp}. In order to better explain the model of the evaporating meniscus, it is advantageous to first discuss the stable isothermal meniscus.

The isothermal extended meniscus

The isothermal, steady state, macroscopic, incompressible energy balance over the distance h above the surface level of the pool is

$$v_l(p_{lp} - p_{lh}) = gh/g_c \tag{2}$$

which gives the decrease in hydrostatic pressure in the nonevaporating extended meniscus. If the vapor is assumed to be an ideal gas, the vapor pressure p_{vh} at any height h above the free bulk surface is given by

$$\mathscr{R}\,T \ln \frac{p_{vh}}{p_{vp}} = -\,g\,hM/g_c. \tag{3}$$

For the intrinsic meniscus portion, the liquid and vapor pressures at h are related by the equation of capillarity

$$p_{lh} = p_{vh} - \sigma_{lv}K_h.$$

These three equations relate the liquid and vapor pressures and curvature at h. As pointed out by Read and Kitchener [9], equations (2) and (3) also apply in the thin film portion except that the pressure difference, $p_{lp} - p_{lh} = -p_d$ is the disjoining pressure which has been measured by Deryagin and others [9, 12]. If the disjoining pressure is negative, (sign convention used by Deryagin) an equilibrium film will adhere to the plate above the intrinsic meniscus decreasing in thickness as the height increases. The disjoining pressure is primarily a function of the film thickness and the nature of the liquid and solid substrate. The various regions of a stable thin film formed on an immersed flat plate have been discussed by Padday [8].

The nonisothermal extended meniscus

The steady state, macroscopic, incompressible energy balance for the increment Δy in Fig. 1 is

$$q J = v\Delta\bar{p} + c\Delta\overline{T} - \Delta\left(\frac{gy}{g_c}\right) + \Delta\left(\frac{\bar{u}^2}{2g_c}\right) \qquad (4)$$

where the individual terms on the right hand side represent the differences occurring over Δy in the average values of the various energies associated with a unit mass of vertically flowing fluid (neglecting at the present time the evaporating portion of the fluid). For the evaporating intrinsic meniscus case, the curvature difference across Δy is greater than that in the isothermal case. This is associated with a larger pressure difference. The additional pressure energy difference gives an increase in thermal energy via viscous dissipation and an increase in kinetic energy. Although the pressure gradient can increase by many orders-of-magnitude as the height decreases, it is interesting to note that the total viscous dissipation is very small.

The thin-film portion of the evaporating extended meniscus consists of evaporating and equilibrium portions. If the height of the plate above the surface of the liquid is sufficiently greater than the height of the intrinsic meniscus, a stable, nonevaporating film of thickness t_0 at its lower limit is adsorbed onto the upper portion of the plate above the evaporating thin film. The surface of the equilibrium film is at a temperature T_{lvo} equal to the plate temperature ($T_{lvo} = T_s > T_v$). However, the thin film does not evaporate because the vapor pressure of the film, p_{vlvo}, is reduced by the disjoining pressure to a value in equilibrium with the local pressure and temperature of the bulk phase. It is assumed here that the top of the evaporating portion of the extended meniscus is close enough to the surface of the pool that changes in the bulk vapor pressure between the pool surface and the top of the intrinsic meniscus may be neglected. The results justify this assumption. The relationship between T_{lvo}, T_v, t_0, has been developed [10, 12].

A short distance below the bottom of the equilibrium film, the film has a thickness $t_h (t_h > t_o)$, and a surface temperature T_{lvh}. ($T_{lvh} < T_p$). Due to the increased thickness, the disjoining pressure of the film is reduced so that $p_{vlvh} > p_{vh}$ in spite of the lower surface temperature and evaporation occurs. The temperature of the film surface is governed by conduction through the film from the heated plate. The rate of evaporation is governed by the film conductance and the interfacial resistance to vapor flow and is a function of t_h, T_{lvh}, T_v, p_{vlvh} and p_{vh}. The model for the intrinsic meniscus is similar to the model for the evaporating portion of the thin film except that the driving force for fluid flow is the gradient of the surface curvature instead of the disjoining pressure.

QUANTITATIVE DESCRIPTION OF THE EXTENDED MENISCUS

The equations which describe the evaporating meniscus fall into three categories: interfacial phenomena, fluid mechanics, and heat transfer. Since the equations describing the latter two are strongly influenced by interfacial phenomena, the equations governing the interface are described first.

Interfacial phenomena

Two of the interfacial phenomena of interest herein, curvature and disjoining pressure, affect both the vapor pressure in equilibrium with the meniscus and the liquid pressure in the meniscus. The effect of curvature on the liquid vapor pressure is given by the well known Kelvin equation

$$\frac{p_{vlv}}{p_{vlvt}} = \exp\left[-\sigma_{lv}KM/\rho_l \mathscr{R}\, T_{lv}\right] \tag{5}$$

where the curvature, K, is positive for the case of a wetting film. The effect of curvature on the liquid pressure is given by equation (4).

A similar effect of the disjoining pressure on the film vapor pressure is developed from the definition of the chemical potential for a pure substance

$$\mu = h - Ts. \tag{6}$$

The change in chemical potential with pressure at constant temperature is

$$\left.\frac{\partial \mu}{\partial p}\right|_T = v. \tag{7}$$

In the liquid, where the density can be taken as constant,

$$\mu_{lL} - \mu_{lo} = v_l(p_{lL} - p_{lo}) = -\frac{Lg}{g_c} \tag{8}$$

where the subscript o refers to the conditions at the lower limit of the equilibrium portion of the thin film. In the vapor, equation (7) becomes for an ideal gas

$$\left.\frac{\partial \mu_v}{\partial p_v}\right|_{T_v} = \frac{\mathscr{R}\, T_v}{M p_v} \tag{9}$$

which leads to the definition of the disjoining pressure at L, p_{dL}

$$\mu_{vL} - \mu_{vo} = \frac{\mathscr{R} T_v}{M} \ln \frac{p_{vL}}{p_{vo}} \equiv \frac{p_{dL}}{\rho_l}. \tag{10}$$

A negative disjoining pressure, p_d, decreases the equilibrium vapor pressure, see equation (2) of [12].

Since the chemical potentials of the two phases (when in equilibrium with each other) must be equal at all heights, their vertical derivatives must also be equal. Equating the derivatives of equations (8) and (10) yields

$$\frac{dp_{lL}}{dL} = \frac{dp_{dL}}{dL} = \frac{\mathscr{R} T_v \rho_l}{M p_{vL}} \frac{dp_{vL}}{dL}. \tag{11}$$

Thus, the pressures in both phases are known as a function of height from a reference point of known pressures. In addition, the gradient of the liquid pressure is equal to the disjoining pressure gradient.

Since the disjoining pressure for a given liquid–solid system is primarily a function of film thickness [20], t, it is convenient to rewrite equation (11) as

$$\left(\frac{dp_d}{dt}\right)\left(\frac{dt}{dL}\right) = -\left(\frac{dp_d}{dt}\right)\tan\theta = -\frac{\rho_l g}{g_c}. \tag{12}$$

Since the film is thin and sufficiently steep so that $\tan\theta \simeq \theta$, equation (12) becomes

$$\theta = \frac{\rho_l g}{g_c(dp_d/dt)}. \tag{13}$$

Anticipating the use of the data of (12), which indicates that the disjoining pressure for non-polar liquids decreases steadily to zero in a manner qualitatively predictable from London's theory of dispersion forces, we assume a functional dependence of p_d on t in the form

$$p_d = -At^{-B}. \tag{14}$$

Using equation (14), equation (13) becomes

$$\theta = \frac{\rho_l q t^{(B+1)}}{A B g_c} \tag{15}$$

and equation (12) can be integrated to yield

$$t_L = \left(\frac{1}{t_0^B} + \frac{\rho_l L g}{g_c A}\right)^{-1/B}. \tag{16}$$

The above derivation assumes a constant temperature in each of the phases but does not require that the temperature of the two phases be equal. This results from the concept that the

chemical potential of the thin layer is a function of its thickness. Disjoining pressure data (12) is taken in an equilibrium system with respect to mass transfer in which the vapor pressure of the film equals the surrounding pressure. However, the temperature of the liquid film is higher than the saturation temperature of the surrounding vapor. Equations (15) and (16) completely define the shape of the nonevaporating portion of either the isothermal or non-isothermal thin film.

The effect of disjoining pressure on the vapor pressure of the film is specified by equation (10). It has been suggested [8] that the effects of disjoining pressure and curvature on the film vapor pressure may be additive with the result that

$$\frac{p_{vlv}}{p_{vlvt}} = \exp\left[\frac{(p_d - \sigma_{lv}K)\,M}{\rho_l \mathscr{R} T_{lv}}\right]. \tag{17}$$

This form of the equation allows a smooth transition from the curvature controlled region to the disjoining pressure controlled region.

Fluid mechanics

A cross-sectional drawing of an evaporating meniscus which includes the nomenclature used in the following analysis is presented in Fig. 1. First, the equation for the pressure gradient in the meniscus at location i will be developed using the assumption that it is equal to that in fully developed flow in the wedge formed by the y coordinate and the tangent to the curve at i. The use of a new center of cylindrical coordinates for each increment of the flow field minimizes the error due to θ-direction flow in the subsequent numerical analysis. The initial portion of the following wedge flow analysis is due to Sparrow and Starr [21]. The results also describe one-half of the symmetrical flow between two flat converging walls.

The mass and momentum conservation laws for fully developed radial flow written in cylindrical coordinates are:

$$\frac{\partial u}{\partial r} + \frac{u}{r} = 0 \tag{18}$$

$$u\frac{\partial u}{\partial r} = -\frac{g_c}{\rho}\frac{\partial P}{\partial r} + \nu\left[\frac{\partial^2 u}{\partial r^2} + \frac{1}{r}\frac{\partial u}{\partial r} - \frac{u}{r^2} + \frac{1}{r^2}\frac{\partial^2 u}{\partial \varphi^2}\right] \tag{19}$$

$$-\frac{g_c}{\rho r}\frac{\partial P}{\partial \varphi} + \frac{2\nu}{r^2}\frac{\partial u}{\partial \varphi} = 0. \tag{20}$$

In accordance with the Jeffery–Hamel analysis, the mass conservation equation is satisfied by the similarity-type solution of the form

$$u = \frac{\nu F(\varphi)}{r}. \tag{21}$$

Substituting equation (21) into equation (20) and then integrating the result at constant r, gives

$$\frac{P}{\rho} = \frac{2\nu^2 F}{r^2 g_c} + \frac{\zeta(r)}{\rho}. \tag{22}$$

Combining equations (19), (21) and (22), results in

$$\frac{\mathrm{d}^2 F}{\mathrm{d}\varphi^2} + 4F + F^2 = \left(\frac{g_c r^3}{\rho \nu^2}\right)\frac{\mathrm{d}\zeta}{\mathrm{d}r} = \text{const.} \tag{23}$$

Sparrow and Starr then linearized equation (23) as follows:

$$\frac{\mathrm{d}^2 F}{\mathrm{d}\varphi^2} + 4F + \varepsilon \bar{F} F = C \tag{24}$$

in which

$$\bar{F} = \frac{1}{\theta}\int_0^\theta F\,\mathrm{d}\varphi. \tag{25}$$

Values of the constant ε, a weighting factor for the mean velocity, are given by Sparrow and Starr [21]. The no-slip boundary conditions for viscous flow on the boundary walls are (symmetrical about $\varphi = 0$).

$$F(\theta) = F(-\theta) = 0. \tag{26}$$

Using these boundary conditions, the solution to equation (24) for the velocity in a converging

plane-walled passage with the half-taper angle θ_i, is

$$u(r_i, \xi) = \frac{\bar{u}_i[\cos\lambda_i - \cos\lambda_i\xi]}{[\cos\lambda_i - (1/\lambda_i)\sin\lambda_i]} \quad (27)$$

in which

$$\xi = \frac{\varphi}{\theta_i}, \qquad \lambda_i = \left(\left|4 + \frac{\varepsilon Re_i}{2\theta_i}\right|\right)^{\frac{1}{2}}\theta_i$$

and

$$Re_i = \left(\frac{\bar{u}\,2\theta r}{\nu}\right)_i, \qquad \bar{F} = \left(\frac{Re}{2\theta}\right)_i.$$

Their results can also be used to obtain equation (28) which relates the velocity to the pressure gradient.

$$u(r, \xi) = \frac{\bar{u}\lambda^2\cos\lambda}{4\theta^2(\cos\lambda - (1/\lambda)\sin\lambda)} - \frac{r^2 g_c}{4\rho\nu}\frac{\partial P}{\partial r}. \quad (28)$$

Equations (27) and (28) are combined to give

$$\bar{u}_i = \frac{z_i^2\,(\partial P/\partial r)_i\,[\cos\lambda_i - (1/\lambda_i)\sin\lambda_i]\,g_c}{\rho\nu\cos^2\theta_i\,[(\varepsilon Re/2\theta_i)\cos\lambda_i + 4]}. \quad (29)$$

Equation (29) relates the average velocity in the wedge to the pressure derivative at the liquid–vapor interface, which is also taken to be the pressure derivative in the meniscus at location i at the interface. In the evaporating thin film this pressure derivative is just that portion of the disjoining pressure gradient available to cause fluid flow.

Taking the surface tension to be a function of temperature only, the normal and shear components of the stress tensor representing the local stress on the liquid at the interface ($\varphi = 0$) of the intrinsic meniscus for a constant $R = R_i$ surface are

$$p_g = -K\sigma_{lv}, \quad \tau_{R\alpha} = -\frac{\beta}{R}\left(\frac{\partial T}{\partial\alpha}\right) = \beta\frac{\partial T}{\partial r} \quad (30)$$

where

$$K = \frac{1}{R}, \; p_g = p_l - p_{vp} \text{ and } \beta = \frac{d\sigma_{lv}}{dT}.$$

The curvature of the meniscus at location i is

$$K_i = \left(\frac{\partial\theta}{dS}\right)_i = \left[\frac{(d^2t/dy^2)}{[1 + (dt/dy)^2]^{\frac{3}{2}}}\right]_i. \quad (31)$$

At equilibrium $p_g = -\rho g h/g_c$, $K_i = \rho g h_i/\sigma_{lv}g_c$ and $(dp_g/\partial r)_i = \rho g\cos\theta_i/g_c$. With evaporation, $p_g < -\rho g h/g_c$ as a result of the additional pressure gradient required to balance liquid acceleration and viscous shear stresses. Since the pressure in the liquid at the liquid–vapor interface of the intrinsic meniscus is a function of the curvature, $p_g|_i = -K_i\sigma_{lv} < -\rho g h/g_c\, i$ when there is evaporation. Using equation (31) with the modified pressure $P = p_g + \rho g h/g_c$

$$\left(\frac{\partial P}{\partial r}\right)_i = -\left[\frac{\partial}{\partial r}\left\{\frac{\sigma_{lv}(d^2t/dy^2)}{[1 + (dt/dy)^2]^{\frac{3}{2}}} - \frac{\rho g h}{g_c}\right\}\right]_i. \quad (32)$$

Equation (32) gives the radial derivative of the pressure at the intrinsic meniscus surface as a function of the meniscus profile. Neglecting thermocapillary flow, equation (32) can now be used with equation (29) to relate the local average velocity, $\bar{u}_i$, to the local intrinsic meniscus profile. The effect of interfacial shear stress due to the temperature gradient will be discussed below.

Heat transfer

The local heat flux across the meniscus is assumed to be fixed by the sum of two resistances: the thermal resistance of the liquid; and the resistance at the liquid–vapor interface to the net flow of vapor. Assuming that the heat flux in the liquid is primarily by conduction in a direction perpendicular to the plate surface, the heat flux across the liquid can be determined using

$$Q = \frac{k}{t}(T_s - T_{lv}). \quad (33)$$

This results from the presence of negligible viscous dissipation and the fact that

$$\frac{\partial T}{\partial r} \ll \frac{1}{r}\frac{\partial T}{\partial\theta}.$$

The interfacial resistance to evaporation from the film yields the following equation for heat flux derived in (1)

$$Q = Hw = \left(\frac{2\sigma H}{2-\sigma}\right)\left(\frac{Mg_c}{2\pi\mathscr{R}}\right)^{\frac{1}{2}}\left(\frac{p_{vlv}}{\sqrt{T_{lv}}} - \frac{p_v}{\sqrt{T_v}}\right) \quad (34)$$

where p_{vlv} is the pressure of the vapor at the liquid–vapor interface and $T_{lv} > T_v$ in the non-isothermal case.

Near the base of the meniscus where the disjoining pressure and curvature have a negligible effect on the vapor pressure of the film, the Clausius–Clapeyron equation gives

$$\ln\frac{p_{vp}}{p_{vlv}} = -\frac{HMJ}{\mathscr{R}}\frac{1}{T_v} - \frac{1}{T_{lv}} \quad (35)$$

or

$$p_{vp} - p_{vlv} \simeq H\bar{p}(T_v - T_{lv})JM/\mathscr{R}T_vT_{lv} \quad (36)$$

where

$$\bar{p} = \frac{p_{vp} + p_{vlv}}{2}.$$

Assuming that equation (34) can be approximately rewritten in the range of interest as

$$Q = \left(\frac{2\sigma H}{2-\sigma}\right)\left(\frac{Mg_c}{2\pi\mathscr{R}\bar{T}}\right)^{\frac{1}{2}}(p_{vlv} - p_v) \quad (37)$$

where

$$\bar{T} = (T_v + T_{lv})/2$$

substitution of equation (36) with $p_{vp} = p_v$ yields

$$Q = \left(\frac{2\sigma H^2}{2-\sigma}\right)\left(\frac{g_c}{2\pi}\right)^{\frac{1}{2}}\left(\frac{M}{\mathscr{R}}\right)^{\frac{3}{2}}\left(\frac{1}{\bar{T}}\right)^{\frac{5}{2}}\bar{p}\,J(T_{lv} - T_v) \quad (38)$$

or

$$Q = h_{\text{evap}}(T_{lv} - T_v). \quad (39)$$

Equations (33) and (39) having only two unknowns can be solved for Q and T_{lv} for known t, T_v and T_s.

Equations (33) and (37) remain valid when either the disjoining pressure and/or the curvature inhibit the evaporation process by reducing the vapor pressure of the film. Using equation (17) for the pressure, p_{vlv}, in equation (37), the system of equations (33) and (37) determine the heat flux and liquid–vapor interfacial temperature if t, T_s, T_{lv}, p_d and K are known.

NUMERICAL

Using a finite difference technique with a given set of parameters (T_v, T_s, p_v, p_d vs. t date) the above equations are sufficient to calculate the extended meniscus profile if the curvature boundary conditions at the top and bottom of the intrinsic meniscus are known.

$$\text{B.C. 1} \quad K = K_t \quad \theta = \theta_t \quad y = Y_t \quad (40)$$

$$\text{B.C. 2} \quad K = K_b \quad \theta = 90 \quad y = Y_. \quad (41)$$

In the present case, the effect of evaporation on the meniscus profile is significant only at small angles. However, continuing the analysis until $\theta = 90°$, allows the use of the boundary condition at the base of the meniscus ($K_b = 0$, $\theta = 90°$) to select the correct curvature at the junction of the thin film and intrinsic meniscus. In the calculation procedure, various initial curvatures are tried until the resulting curvature becomes zero at the base. The pressure drop required for fluid flow in the intrinsic meniscus comes from only this curvature change.

In the thin film portion of the extended meniscus, the pressure drop comes from only the change in the disjoining pressure. The disjoining pressure versus thickness data for carbon tetrachloride on a smooth glass surface [12] used in the calculations are presented in Fig. 2. As shown in the figure, the data can be represented by two line segments for the purpose of convenience yielding the following value of the constants defined in equation (14):

	$t < 7{\cdot}28 \times 10^{-7}$cm	$t > 7{\cdot}28 \times 10^{-7}$cm
A	282·5	$0{\cdot}609 \times 10^{-12}$
B	0·61	3·0

Although the discontinuous slope does effect the calculations, sufficient accuracy is main-

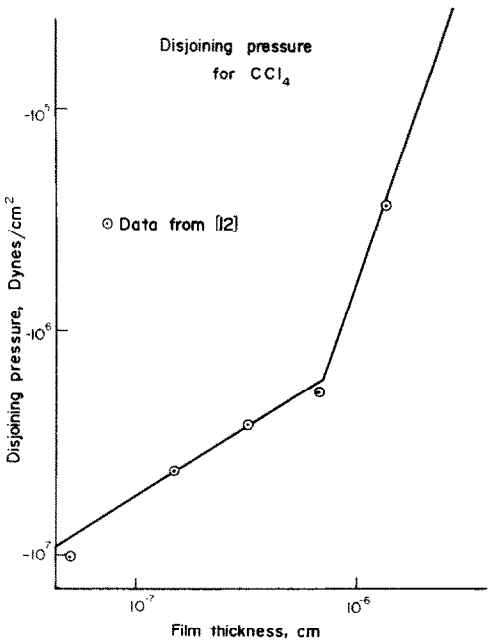

FIG. 2.

tained for the present calculations. It should be noted that a slope of $-3{\cdot}0$ for "thick films" is theoretically predictable from consideration of the London forces in a non-polar liquid [20] and is therefore used in this region. The more shallow slope of $-0{\cdot}61$ for the remainder of the thin film is the best fit to the data.

Isothermal meniscus

For the isothermal case ($T_v = T_s = 293°K$) equations (15) and (16) are used to calculate the thin film profile. The junction of the thin film and intrinsic meniscus is taken to be that point where the pressure change due to capillarity becomes greater than the disjoining pressure. Using the Euler finite difference approximation for curvature, equation (32) is used to calculate the isothermal intrinsic profile with the modified pressure, P, equal to zero.

Evaporating meniscus

Since evaporation occurs within the thin film, the calculation for the evaporating extended meniscus starts at the highest point in the thin film at which evaporation occurs ($L = 0$). In this case $T_v = 293°K$. $T_p = 293{\cdot}272°K$. $P_v = 1{\cdot}17 \times 10^5$ dynes/cm^2. The equilibrium thickness just above this point is obtained from Fig. 2 using the local value of the disjoining pressure which is obtained by substituting equation (17) into equation (37). The heat flux and curvature at the bottom of the equilibrium thin film are equal to zero. The wedge angle for the first increment downward is obtained from equation (15). At the bottom of the first increment, $\Delta y = 10$ Å, the film thickness, t_1, is greater than t_0 by an amount equal to $\Delta y \tan\theta$. Knowing the thickness at location 1, the disjoining pressure is obtained from Fig. 2. Knowing the disjoining pressure, the film vapor pressure and heat flux are obtained using equations (17) and (37) initially assuming that the liquid–vapor interfacial temperature remains constant over Δy. The required interfacial temperature is then obtained from equation (33) using the calculated heat flux and the above procedure is repeated until there is a negligible change in the interfacial temperature. The evaporation coefficient is taken to be unity. The average velocity of the fluid entering the first increment is then obtained from the average surface flux assuming that all the fluid entering the first increment is evaporated. Knowing the average velocity, the pressure gradient at $i = 1$ is obtained using equation (29). The disjoining pressure gradient is equal to the sum of the pressure gradient for fluid flow and the weight density. Using this disjoining pressure gradient, a new wedge angle, thickness, heat flux, total fluid flow and new pressure gradient at the bottom of the second increment are calculated using Fig. 2 and equations (13), (15), (33), (37) and (29). This is continued until the film becomes sufficiently thick and the disjoining pressure has a negligible effect on the heat flux. At this point the intrinsic meniscus starts. The average velocity, heat flux, pressure gradient and wedge angle are continuous across the transition into the intrinsic meniscus.

The total fluid flow leaving the intrinsic meniscus and the initial angle and thickness of

the intrinsic meniscus are known. A value of the curvature at this point is now assumed since its value depends on the boundary condition at the bottom of the meniscus. With the initial angle and assumed initial curvature. the slope of the intrinsic meniscus a distance Δy down from the top is calculated using the Euler finite difference approximation of the curvature. equation (31). The change in meniscus thickness is the product of the step size and the average slope of the wedge. The heat flux over the increment is calculated from equations (33) and (39). The volumetric flow entering the bottom of the wedge. being equal to the total fluid evaporated above the wedge plus the fluid evaporated from the wedge. is calculated. The pressure derivative is then calculated from equation (29) and the change in curvature from the finite difference approximation of equation (32). Using Euler's method. this process is continued until the wedge angle equals ninety degrees. As in the case of the isothermal intrinsic meniscus. various values of the initial curvature are tried until the boundary condition $K = 0$ at $\theta = 90°$ is satisfied.

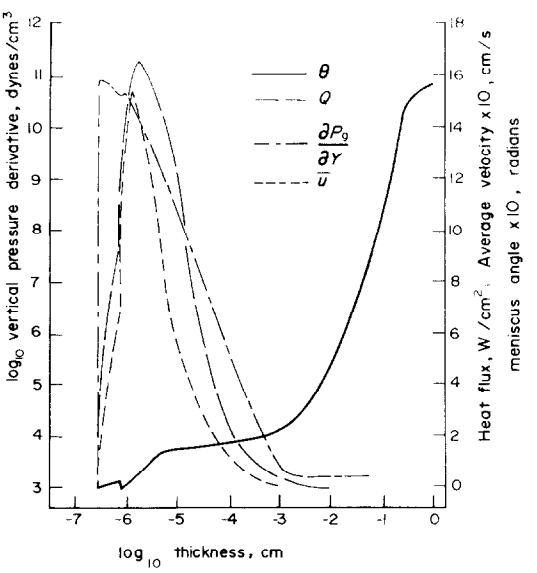

FIG. 3.

RESULTS

The heat flux. vertical pressure derivative. wedge angle and average velocity are plotted versus the meniscus thickness in Fig. 3. The discontinuous slopes at $t = 7{\cdot}28 \times 10^{-7}$ cm are due to the approximation of the data. For all practical purposes. the results could be smoothed in this region. The heat flux and velocity are zero at $t = t_0 = 23{\cdot}9$ Å which is the bottom of the nonevaporating. non-isothermal thin film. Above this point. there is a hydrostatic decrease in pressure. The velocity. pressure derivative and heat flux reach a maximum in the evaporating thin film portion of the extended meniscus. After this point. the thin film becomes sufficiently thick that the heat flux. velocity and pressure derivative decrease in magnitude. The length of the evaporating thin film portion is 13 950Å. The thickness of the thin film at its junction with the intrinsic meniscus is 344 Å The height of the intrinsic meniscus is 0·1711 cm. The heat flux and velocity decrease to zero at the bottom of the intrinsic meniscus. It is interesting to note that the dimensions of the evaporating thin film and upper portion of the intrinsic meniscus are compatible with porous media heat exchangers. More significantly, the results demonstrate that the model allows for a smooth transition between an adsorbed non-evaporating thin film and an evaporating meniscus.

In Fig. 4. the isothermal and non-isothermal menisci profiles are presented. The discontinuities in the slopes are due to an abrupt switch from one model to another. This could be smoothed by using additional data and a transition region model that includes disjoining pressure and capillarity. The left hand vertical scale covers the entire extended meniscus profile. The right hand vertical scale covers only a portion of the extended meniscus. The height of the isothermal intrinsic meniscus is 0·1844 cm. whereas the height of the evaporating intrinsic meniscus is 0·1711 cm. This decrease

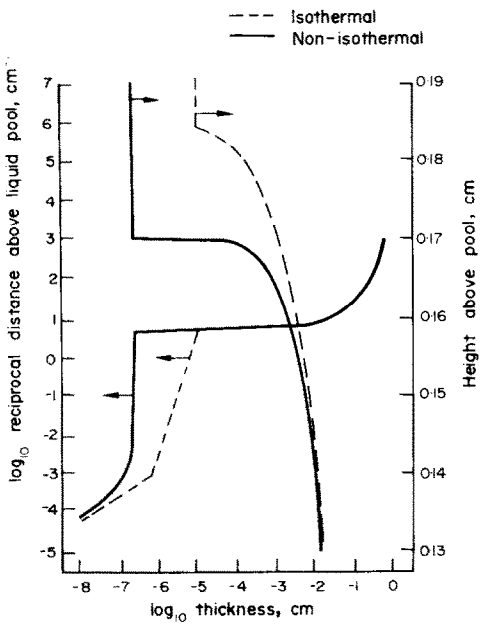

FIG. 4.

in height provides the increased curvature gradient needed to balance the viscous stresses in the intrinsic meniscus. As shown in Fig. 4. the thickness of the non-isothermal meniscus is less than that of the isothermal meniscus for the same height. This results from the larger pressure drop in the non-isothermal meniscus (at the top of the evaporating thin film. a height of 0·1712395 cm above the pool. $P_d = -3{\cdot}09 \times 10^6$ dynes/cm^2. whereas the pressure drop in the isothermal meniscus at this height is only 268 dynes/cm^2). A pressure drop of $3{\cdot}09 \times 10^6$ dynes/cm^2 is equal to the hydrostatic pressure drop in a column of carbon tetrachloride 1976 cm high. This suction potential (less the negligible portion associated with the intrinsic meniscus) is used over a very short distance (13950Å) to balance the viscous stresses in the evaporating thin film.

DISCUSSION

The above analysis is based on the premise that a fully developed wedge flow model can be used in the meniscus. A partial feeling for the correct velocity distribution can be obtained from a boundary layer calculation of the distance required for the boundary layer thickness for flow over a flat plate to be equal to 1×10^{-3} cm. This is the approximate thickness of the meniscus in the region where viscous effects become negligible. A simple form of the boundary layer equation is

$$x = \frac{t^2 u_\infty}{30\nu}. \tag{42}$$

Using the interfacial velocity at $t = 1 \times 10^{-3}$ cm for u_∞. the calculated distance is negligible compared to the distance from the bottom of the plate to this point. In fact the velocity is so low and thickness small, that the use of the simple form of the boundary layer equation is not justified. However. the large difference between these two distances definitely indicates that the accelerating velocity profile is well developed in and above this region. In addition. since the angle θ_i is still small in this region. θ-direction flow has a small effect on the meniscus profile. These two results indicate that the wedge flow model is a good approximation to the flow field in the upper portion of the meniscus. Since viscous effects become negligible below this region. the continued use of the model does not affect the validity of the rest of the profile. In addition. the evaporation process. which is a relatively small change from dynamic equilibrium. is not expected to strongly affect this flow model (except for thermocapillary flow).

The thermocapillary shear stress at the liquid–vapor interface is assumed to be negligible in the present analysis. This assumption is based on the results of [7] which demonstrated that the thermocapillary effect in the upper portion of the meniscus was small compared to the curvature effect. Thermocapillary flow would have an effect on the profile in the lower and less important portion of the meniscus. However. inclusion of this effect requires *a priori* knowledge of the temperature gradient. Since this gradient is unknown. its inclusion

would require an additional set of iterations which is beyond the scope of the present study.

All calculations begin at the bottom of the equilibrium portion of the thin film. Therefore, the initial height of this point above the pool is not known. For this reason, the bulk vapor pressure at the level of the intrinsic meniscus and the evaporating portion of the thin film is also not known and is assumed to be a constant equal to the thermodynamic saturation pressure at T_v. This gives an artificial start to the evaporation process at t_0 since the disjoining pressure is allowed to vary. This artifice is justified by the small calculated height of the evaporating portion of the extended meniscus and, therefore, relatively small change in the real bulk vapor pressure. On the other hand, the large viscous stresses associated with fluid flow in a very thin film result in very large changes in the disjoining pressure and the thin film vapor pressure which quickly minimizes the error. For the equilibrium thin film portion of the meniscus, the vapor pressure is allowed to vary. In order to write the heat transfer equation at the liquid–vapor interface in simple form the Clasius–Clapeyron equation and the assumption that

$$\frac{P_v}{\sqrt{T_v}} - \frac{p_{vlv}}{\sqrt{T_{lv}}} = \frac{P_v - p_{vlv}}{\sqrt{\bar{T}}}$$

were used. For the very small temperature difference involved, the decrease in accuracy resulting from these assumptions is relatively small. Throughout the above described calculations, bulk fluid properties for 20°C and Newtonian flow were assumed applicable. Insufficient data concerning the transport properties in adsorbed films is presently available to do otherwise.

CONCLUSIONS

1. The pressure drop resulting from a change in the extended meniscus profile is sufficient to give the fluid flow required for evaporation.
2. The evaporating portion of an extended wetting meniscus consists of both an evaporating intrinsic meniscus in which fluid flow partially results from capillarity and an evaporating thin film in which fluid flow results from the disjoining pressure gradient.
3. The velocity and heat flux profiles for a stable evaporating carbon tetrachloride extended meniscus formed on a semi-immersed superheated (0·5°F) smooth flat glass plate start at zero where the thickness is 23·9 Å, go through a maximum value and then return to a negligible value when the meniscus becomes relatively thick.
4. The full extent of the evaporating thin film is compatible with the dimensions of porous media heat transfer devices.

ACKNOWLEDGEMENT

This research was partly supported by the Department of the Army Contract No. DAAB07-69C0063 entitled "Electrochemical Power Sources". A preliminary version of this paper (Reprint #14a) was presented at the 70th Annual Meeting of A.I.Ch.E. in Atlantic City, New Jersey, 29 August–1 September, 1971.

REFERENCES

1. S. P. SUKATME and W. M. ROHSENOW, Heat transfer during film condensation of a liquid metal vapor, *J. Heat Transfer* **88C**, 19–28 (1966).
2. K. NABAVIAN and L. A. BROMLEY, Condensation coefficient of water, *Chem. Engng Sci.* **18**, 651–660 (1963).
3. A. UMUR and P. GRIFFITH, Mechanism of dropwise condensation, *J. Heat Transfer* **87C**, 275–282 (1965).
4. R. W. SCHRAGE, *A Theoretical Study of Interphase Mass Transfer*. Columbia University Press, New York, N.Y. (1953).
5. R. G. BRESSLER and P. W. WYATT, Surface wetting through capillary grooves, *J. Heat Transfer* **92C**, 126–132 (1970).
6. P. C. WAYNER, JR. and C. L. COCCIO, Heat and mass transfer in the vicinity of the triple interline of a meniscus, *A.I.Ch.E.Jl* **17**, 569–574 (1971).
7. P. C. WAYNER, JR. and M. POTASH, JR., Fluid flow in an evaporating meniscus, Preprint #30b, 63rd Annual Meeting, A.I.Ch.E., Chicago, Ill. 29 Nov.–3 Dec., (1970.
8. J. F. PADDAY, Cohesive properties of thin films on liquids adhering to a solid surface, Preprint #6. Special Discussion, Faraday Society, Cambridge (Sept. 1970).
9. A. D. READ and J. A. KITCHENER, The thickness of wetting films S.C.I Monograph No. 25 on Wetting, p. 300, Soc. Chem. Ind., London (1967).

10. B. V. DERYAGIN and L. M. SHCHERBAKOV, Effect of surface forces on phase equilibria of polymolecular layers and contact angle, *Colloid J., U.S.S.R.* (trans.) **23**, 33–43 (1961).
11. A. SHELUDKO, *Colloid Chemistry*, p. 173. Elsevier, Amsterdam (1966).
12. B. V. DERYAGIN and A. M. ZORIN, Optical study of the adsorption and surface condensation of vapors in the vicinity of saturation on a smooth surface, Proc. 2nd Int. Congr. Surface Activity (London), **2**, pp. 145–152 (1957).
13. L. E. SCRIVEN, Dynamics of a fluid interface, *Chem. Engng Sci.* **12**, 98–108 (1960).
14. C. V. STERNLING and L. E. SCRIVEN, Interfacial turbulence: hydrodynamic instability and the marangoni effect, *A.I.Ch.E.Jl* **5**, 514–523 (1959).
15. J. J. LORENZ and B. B. MIKIC, The effect of thermocapillary flow on heat transfer in dropwise condensation, *J. Heat Transfer* **92C**, 46–52 (1970).
16. E. N. LIGHTFOOT and V. LUDVIKSSON, Electrochemical processes in thin films, *J. Electrochem. Soc.* **113**, 1325–1329 (1966).
17. YU. A. CHIZMADZHEV and V. S. MARKIN, The nature of films of liquid on semi-immersed electrodes, *Elektrokhimiya* **2**, 1360–1362 (1966).
18. YU. G. CHIRKOV, V. S. MARKIN and V. S. CHESNOKOV, Theory of the liquid film on partly immersed electrode in the absence of electrical currents, *Elektrokhimiya* **6**, 889–904 (1970).
19. B. V. DERYAGIN, S. V. NERPIN and N. V. CHURAYEV, Effect of film transfer upon evaporation of liquids from capillaries, Bulletin Rilem No. 29, 93–98 (1965).
20. A. SHELUDKO, Op. Cit. p. 176.
21. E. M. SPARROW and J. B. STARR, Heat transfer to laminar flow in tapered passages, *J. Appl. Mech.* **32E**, 684–689 (1965).

EVAPORATION A PARTIR D'UN MENISQUE ETENDU BIDIMENSIONNEL

Résumé—On a analysé sur un modèle les processus de transport au cours de l'évaporation d'un ménisque bidimensionnel et d'un film mince adsorbé formé sur une plaque plane de verre surchauffée (0,272°C de surchauffe) immergée dans un réservoir de tétrachlorure de carbone saturé. L'écoulement fluide résulte d'un changement du profil externe du ménisque. Le gradient de pression pour l'écoulement fluide comprend l'effet de pression de disjonction. Le profil du ménisque étendu résultant, le profil du flux thermique et le profil de pression sont calculés. La présence d'un film surchauffé adsorbé se traduit par une transition douce entre les états d'évaporation et de non-évaporation du ménisque.

VERDAMPFUNG VON EINEM ZWEIDIMENSIONALEN MENISKUS

Zusammenfassung—Zur Analyse der Transportvorgänge in einem zweidimensionalen Meniskus bei Verdampfung und einem adsorbierten Dünnfilm auf einer überhitzten flachen Glasplatte (0,272°C Überhitzung), die in einen Behälter mit gesättigtem Tetrachlorkohlenstoff eingetaucht war, wurde ein Modell aufgestellt.

Die Flüssigkeitsströmung rührt von einer Änderung in dem äusseren Meniskusprofil her. Der Druckgradient für die Flüssigkeitsströmung berücksichtigt auch den Zugeinfluss. Das resultierende Meniskusprofil, die Wärmestrom- und Druckverteilung werden berechnet. Die Anwesenheit eines adsorbierten überhitzten Films führt zu einem glatten Übergang zwischen den verdampfenden und nichtverdampfenden Anteilen des Meniskus.

ИСПАРЕНИЕ С ДВУХМЕРНОГО ВЫТЯНУТОГО МЕНИСКА

Аннотация—Моделируются и анализируются процессы переноса, происходящие в испаряющемся двухмерном мениске и адсорбированной тонкой пленке, образованной на перегретой плоской стеклянной пластине (перегрев 0,272°C), погруженной в резервуар с насыщенным четыреххлористым углеродом. Течение жидкости вызывается изменением внешнего профиля мениска. Градиент давления для жидкого потока включает эффект давления разъединения. Рассчитываются профиль вытянутого мениска, профиль теплового потока и профиль градиента давления. Наличие адсорбированной перегретой пленки приводит к плавному переходу между испаряющимся и неиспаряющимся участками вытянутого мениска.